Conformational Flexibility of the Acetylcholinesterase Tetramer Suggested by X-ray Crystallography*

Yves Bourne, Jacques Grassi, Pierre E Bougis, Pascale Marchot

THE JOURNAL OF BIOLOGICAL CHEMISTRY
Vol. 274, No. 43, Issue of October 22, pp. 30370–30376, 1999
Printed in U.S.A.

Conformational Flexibility of the Acetylcholinesterase Tetramer Suggested by X-ray Crystallography*

(Received for publication, March 29, 1999, and in revised form, July 26, 1999)

Yves Bourne‡, Jacques Grassi§, Pierre E. Bougis¶, and Pascale Marchot¶‖

From the ‡CNRS, Unité Propre de Recherche 9039, Architecture et Fonction des Macromolécules Biologiques, Institut de Biologie et Microbiologie Structurale, F-13402 Marseille cedex 20, France, §Commissariat à l'Energie Atomique, Service de Pharmacologie et d'Immunologie, Département de Recherches Médicales, Commissariat à l' Energie Atomique-Saclay, F-91191 Gif sur Yvette Cedex, France, and ¶CNRS, Unité Mixte de Recherche 6560, Ingénierie des Protéines, Institut Fédératif de Recherche Jean Roche, Université de la Méditerranée, F-13916 Marseille cedex 20, France

Acetylcholinesterase, a polymorphic enzyme, appears to form amphiphilic and nonamphiphilic tetramers from a single splice variant; this suggests discrete tetrameric arrangements where the amphipathic carboxyl-terminal sequences can be either buried or exposed. Two distinct, but related crystal structures of the soluble, trypsin-released tetramer of acetylcholinesterase from *Electrophorus electricus* were solved at 4.5 and 4.2 Å resolution by molecular replacement. Resolution at these levels is sufficient to provide substantial information on the relative orientations of the subunits within the tetramer. The two structures, which show canonical homodimers of subunits assembled through four-helix bundles, reveal discrete geometries in the assembly of the dimers to form: (*a*) a loose, pseudo-square planar tetramer with antiparallel alignment of the two four-helix bundles and a large space in the center where the carboxyl-terminal sequences may be buried or (*b*) a compact, square nonplanar tetramer that may expose all four sequences on a single side. Comparison of these two structures points to significant conformational flexibility of the tetramer about the four-helix bundle axis and along the dimer-dimer interface. Hence, in solution, several conformational states of a flexible tetrameric arrangement of acetylcholinesterase catalytic subunits may exist to accommodate discrete carboxyl-terminal sequences of variable dimensions and amphipathicity.

Differences in the molecular forms of the cholinesterases are the primary determinants of their tissue distribution and disposition within a cell; association of subunits also may govern the turnover of the enzyme (*cf.* Refs. 1 and 2). In mammals, the predominant form of acetylcholinesterase (AChE)[1] in the central nervous system is an amphiphilic tetramer anchored to the membrane by a hydrophobic, noncatalytic subunit; at the neuromuscular junction, it is an asymmetric form containing 1–3 tetramers associated with the basal lamina by a collagen-like, structural subunit. Collagen-tailed forms are also predominant in the electric organ of the eel *Electrophorus electricus*. In the form containing three catalytic tetramers, three collagen-like subunits are disulfide-linked together, and each is attached to a tetramer in which two catalytic subunits forming a proximal dimer are disulfide-linked to the tail subunit and are associated with a peripheral dimer by quaternary interactions (3, 4) (Scheme 1).[2] Apart from the association as a dimer of disulfide-linked dimers, both amphiphilic and nonamphiphilic tetramers appear to form from a single splice variant. The eel $AChE_T$ subunits (EeAChE) present the capacity to form heteromeric quaternary associations (5). This suggests discrete tetrameric arrangements where the amphipathic carboxyl-terminal sequences (T peptides) are either buried or exposed.

Tetrameric arrangements of AChE subunits were observed *in situ* (6–8), and several models were proposed (4, 9–11); however, little structural information is available about the subunit orientation in the tetramer and the association of tetramers with anchor subunits. The crystal structure of recombinant mouse AChE (mAChE) revealed a compact, pseudo-square planar tetrameric arrangement of subunits (12); mAChE, however, lacks the carboxyl-terminal hydrophobic glycophospholipid or the amphipathic helix found on natural forms of AChE and is expressed as a monomer (13), a feature that poses the question of whether physiological forms of the enzyme would form a similar tetramer. In fact, crystals of EeAChE and diffraction experiments were reported earlier (14–16), but solution of a structure was precluded by the limited resolution achieved and failure in obtaining heavy atom derivatives, along with unavailability of a three-dimensional template for molecular replacement and of the primary structure of the eel species. Since then, crystal structures of *Torpedo californica* AChE (TcAChE) (17) and mAChE (18) were solved, and the cDNA-derived primary structure of EeAChE was determined (5).

Here we report two low resolution crystal structures solved from two distinct crystal forms grown in different conditions from the soluble, trypsin-released EeAChE tetramer. These structures reveal discrete but related tetrameric arrangements of catalytic subunits that are consistent overall with that found in the mAChE crystal and with arrangements observed *in situ*. Moreover, comparison of these arrangements suggests that, in solution, the AChE tetramer has significant conformational flexibility.

* This work was supported by the Association Française contre les Myopathies (to P. E. B. and P. M.) and the Commissariat à l'Energie Atomique (to J. G.). A preliminary report of these structures was presented during the Sixth International Meeting on Cholinesterases and Related Proteins (La Jolla, CA, 1998). The costs of publication of this article were defrayed in part by the payment of page charges. This article must therefore be hereby marked "*advertisement*" in accordance with 18 U.S.C. Section 1734 solely to indicate this fact.

The atomic coordinates (code 1C2B for structure A and code 1C2O for structure B) have been deposited in the Protein Data Bank, Research Collaboratory for Structural Bioinformatics, Rutgers University, New Brunswick, NJ (http://www.rcsb.org/).

‖ To whom correspondence should be addressed: Fax: (33) 4-91-65-75-95; E-mail: marchot.p@jean-roche.univ-mrs.fr.

[1] The abbreviations used are: AChE, acetylcholinesterase; EeAChE, *E. electricus* AChE; mAChE, recombinant mouse AChE; PAGE, polyacrylamide gel electrophoresis; TcAChE, *T. californica* AChE.

[2] Scheme 1 is not intended to describe the crystal structures reported in this study.

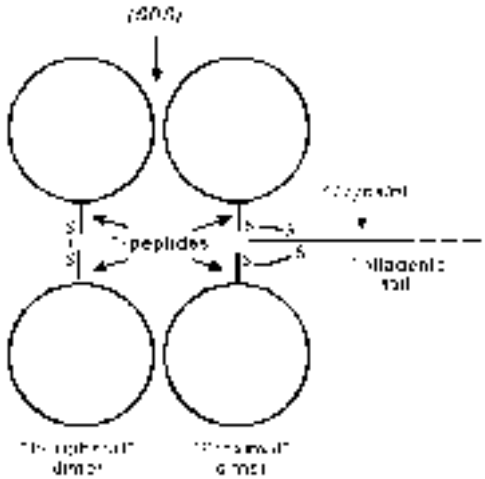

SCHEME 1

EXPERIMENTAL PROCEDURES

Materials—The prepacked Superdex-200 HiLoad 26/60 column and the gel-filtration calibration markers were from Amersham Pharmacia Biotech. *N*-Tosyl-L-phenylalanine chloromethyl ketone-treated trypsin (EC 3.4.21.4) and the protein molecular weight standards for SDS-PAGE were from Sigma. Other reagents and the salts used for crystallization were of the highest grade available.

Purification and Analysis of the Tetramer—EeAChE, as a mixture of asymmetric forms, was isolated from homogenized electric organs by affinity chromatography and subjected to tryptic cleavage as described previously (19). The released tetramer was purified by size-exclusion fast performance liquid chromatography (Amersham Pharmacia Biotech) on a Superdex-200 column equilibrated and eluted with 100 mM $NaKPO_4$, pH 7.5, 400 mM NaCl, 0.01% NaN_3 (w/v) at a flow rate of 0.5 ml min^{-1} and at 20 °C. The purified tetramer was dialyzed against 100 mM $NaKPO_4$, pH 7.5, 100 mM NaCl, 0.01% NaN_3 (w/v) and concentrated to 10–15 mg ml^{-1}; it was stored on ice.

AChE activity measurements were conducted spectrophotometrically (20) with 0.5 mM acetylthiocholine and 0.33 mM dithiobis(2-nitrobenzoic acid) in 100 mM $NaPO_4$, pH 7.0, 0.1 mg ml^{-1} bovine serum albumin (λ = 412 nm) (13).

SDS-PAGE was performed on homogeneous 7.5% gels using a PhastSystem apparatus (Amersham Pharmacia Biotech). The samples were boiled for 5 min in the presence of 2.5% (w/v) SDS with (reducing conditions) or without (nonreducing conditions) 5% (v/v) β-mercaptoethanol. Staining was by silver nitrate according to the manufacturer's method number 210.

Crystallization and Data Collection—Crystallization was achieved by vapor diffusion using hanging drops of 4 μl and a protein-to-well solution ratio of 1:1. Form A crystals were grown at 4 °C using 1.1–1.5 M $NaKPO_4$, pH 8.0–9.5, as the well solution; form B crystals were grown at 20 °C using 1.4 M ammonium sulfate, pH 5.5–6.0, as the well solution. Data were collected at 20 °C on mounted crystals and using a 300 mm MarResearch imaging plate detector equipped with a Siemens rotating anode (50 kV × 80 mA). Oscillation images were integrated with DENZO (21) and scaled and merged with SCALA (22) (Table I). Amplitude factors were generated with TRUNCATE (23). Form A crystals belonged to the orthorhombic space group F222 with unit cell dimensions a = 118 Å, b = 215.9 Å, c = 229.4 Å, giving a V_m value of 4.5 $Å^3$/Da (73% solvent) for one EeAChE subunit (~80 kDa) in the asymmetric unit (24). Form B crystals belonged to the monoclinic space group C2 with unit cell dimensions a = 211 Å, b = 129.7 Å, c = 195.4 Å (β = 103.2°), giving a V_m value of 4.1 $Å^3$/Da (69.5% solvent) for one EeAChE tetramer (~320 kDa) in the asymmetric unit.

Structure Solution and Refinement—Initial phases for structure A were obtained by molecular replacement using the AChE subunit from the mAChE structure (Protein Data Bank code 1MAA) (12) as a search model with the AMoRe program package (25) (Table I). The phases calculated from a positioned catalytic subunit were improved by solvent flattening using program DM (23) and a mask built around the subunit. The same procedure with additional averaging was used for structure B. For the two structures, rigid body refinement was applied to the whole subunit using the program CNS (26). Accuracy of the structures was further checked by omitting from the starting model and before rigid body calculation the entire 17-residue helix α_{10} (mAChE residues 526–543), a key structure element for the formation of the dimer four-helix bundle (12, 18); difference electron density maps calculated after rigid body refinement unambiguously revealed the presence of helix α_{10} (*cf.* Fig. 4).

Figs. 2, 3, and 4 were generated with the ALSCRIPT (27), RIBBON (28), and TURBO-FRODO (29) programs, respectively.

TABLE I
Data collection and refinement statistics

	Structure A (F222)	Structure B (C2)
Data collection		
Resolution range (Å)	10–4.5	12–4.2
Total observations	101, 833	158, 367
Unique reflections	7, 742	24, 590
Multiplicity	2.9	1.9
Completeness (%)	74	66
R_{sym} (%)[a]	20	18
Structure determination		
AMoRe		
Correlation	57	58
R-factor (%)[b]	49	36.5
DM		
R-factor (%)[c]	36	34
R_{free} (%)[d]	38	36.5
Refinement		
CNS rigid body refinement:		
R-factor (%)[b]	36.9	37.5
R_{free} (%)[d]	35.1	38.5
Map correlation	0.87	0.82

[a] $R_{sym} = \Sigma|I - \langle I\rangle|/\Sigma I$, where I is an individual reflection measurement and $\langle I\rangle$ is the mean intensity for symmetry-related reflections.

[b] *R*-factor = $\Sigma||F_o| - |F_c||/\Sigma|F_o|$, where F_o and F_c are observed and calculated structure factors, respectively.

[c] *R*-factor calculated with SFALL using structure factor and phase informations from DM (*cf.* 23).

[d] R_{free} is calculated for 3% of randomly selected reflections excluded from refinement.

RESULTS AND DISCUSSION

Characterization of the Purified EeAChE Tetramer

The trypsin-released tetramer eluted from the gel filtration column as a single, symmetric absorbance peak of apparent mass of ~360 kDa; analysis of the specific AChE activity throughout the peak suggested functional homogeneity of the tetramer (data not shown). However, electrophoretic analysis suggested structural heterogeneity. Indeed, although SDS-PAGE performed in reducing conditions yielded the three broad bands of ~80, 50, and 30 kDa, characteristic for reduced EeAChE (30, 31), SDS-PAGE performed in nonreducing conditions yielded a weak, thin band of ~320 kDa representing residual tetramer and two pairs of closely migrating, intense bands in a ratio of about 1:1 and average apparent masses of ~160 and 80 kDa, values consistent with dimers and monomers, respectively (Fig. 1). The purified tetramer thus appears not only to be composed of two equal populations of dimers differing slightly in their masses (as expected from a dimer of dimers where one set of disulfides links with the residual tail and the other set forms between monomers; *cf.* Scheme 1) but also to contain, in the same proportion, two equal populations of slightly different monomers. Trypsin cleaves peptides and proteins at the ester linkages of arginines and lysines, two residues that are found upstream of the linking cysteines not only in the amino-terminal end of the tail (32, 33) but also in the carboxyl-terminal end of the EeAChE catalytic subunit (T peptide, Fig. 2) (5). In the presence of SDS, dimers that lack the disulfide dissociate into monomers. Hence, the EeAChE tetramer subjected to crystallization is composed of two equal populations of covalent and noncovalent dimers, either proximal or distal to the tail.

The apparent mass of the EeAChE tetramer estimated from chromatography is ~12% higher than that estimated from

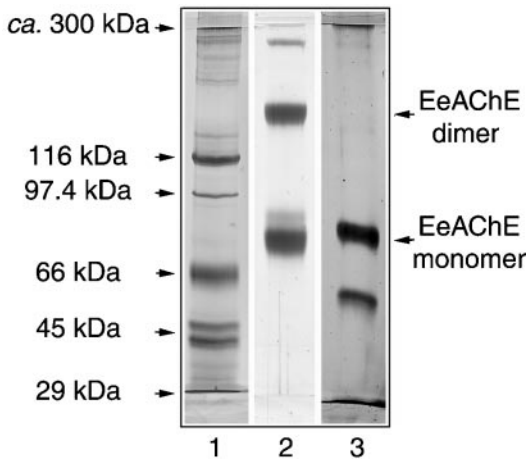

FIG. 1. **Electrophoretic analysis of the purified EeAChE tetramer (SDS-PAGE).** *Lane 1*, molecular mass standards under reducing conditions: β-galactosidase (116 kDa), phosphorylase *b* (97.4 kDa), bovine serum albumin (66 kDa), ovalbumin (45 kDa), and carbonic anhydrase (29 kDa, migrating together with the free SDS at the bottom of the gel). *Lane 2*, the EeAChE tetramer under nonreducing conditions; the broad dimer and monomer bands are resolved as two pairs of closely migrating bands when very low amounts of protein are loaded. *Lane 3*, the EeAChE tetramer under reducing conditions; the 30-kDa band is visible at the bottom of the gel.

electrophoresis, a difference that suggests either dimensional asymmetry or a high level of hydration of the tetramer (or both). Substantial dimensional asymmetry was reported earlier for the EeAChE tetramer (3), the homologous 11S TcAChE species (34), and the fetal bovine serum AChE tetramer (35). Alternatively, two highly solvated crystal forms were grown from the purified EeAChE tetramer (*cf.* "Experimental Procedures").

Tetrameric Arrangements of EeAChE Subunits

For each of the two EeAChE structures herein reported, the low resolution achieved does not reveal details in the positions of the side chains in the catalytic subunit nor in those located at the subunit interfaces. As well, structure elements that are unique to the eel enzyme, peptide Ile^{418}–Gln^{446} and the carboxyl-terminal T peptide Glu^{571}–Leu^{610} (5) (Fig. 2), are not resolved. Yet, each of the structures provides substantial information on the arrangement of the subunits within the tetramer. A single solution was found for the positions and orientations of the subunits in pairs whether molecular replacement used an isolated subunit or a dimer of subunits as a search model. Indeed, dimers of subunits related by four-helix bundles and identical to dimers observed in structures of TcAChE (17, 36) and mAChE (12, 18) were observed. The two EeAChE structures, however, differ in the geometry of the two dimers within the tetramer. Because of the current resolutions, the EeAChE backbone was not modeled, and the backbone shown is that of mAChE. Accordingly, the EeAChE residues are referred to relative to the mAChE backbone based on sequence homology (Fig. 2), and the number in parentheses that follows the EeAChE residue number (5) denotes the corresponding position in mAChE (13, 37).

Structure A—In EeAChE structure A, the two dimers arrange as a loose, pseudo-square planar tetramer of a marked dimensional asymmetry (Fig. 3). The two four-helix bundle axes are aligned antiparallel, and the main axes of the two dimers are tilted by ~40° from each other, a geometry reminiscent of that observed in the mAChE structure (12). At the dimer-dimer interface, which extends over 75 Å in a direction roughly perpendicular to the four-helix bundle axis, loop $Cys^{256(257)}$–$Cys^{267(272)}$, which is located between helices $\alpha^1_{6,7}$ and $\alpha^2_{6,7}$ and protrudes at the surface of each subunit in a dimer (12), is at a near contact distance of 13 Å from the homologous loop in the facing subunit of the second dimer. This loop in EeAChE is shorter by four residues than in mAChE, but the oligosaccharide moieties linked to the facing $Asn^{260(265)}$ residues may interact with each other and lock the arrangement. A similar cross-interaction may occur for the oligosaccharide moieties linked to the facing $Asn^{161(162)}$ residues. The carboxyl-terminal helices α_{10} in the four-helix bundles converge toward the center of the tetramer, but the facing $Thr^{570(543)}$ residues, terminal to helices α_{10}, are separated by 35 Å. As a result, the surface area buried at the dimer-dimer interface does not exceed a few $Å^2$ on each dimer and there is a large space, apparently empty of electron density, at the center of the tetramer.

In tetramer A, the four gorges that lead to the EeAChE active centers are oriented roughly antiparallel in a direction perpendicular to the tetramer plane. All four peripheral sites, of which two, from diagonally opposed subunits, are exposed on one face of the tetramer and two on the other face, are freely accessible to the solvent, a geometry consistent with the binding of four fasciculin or inhibitory antibody molecules/AChE tetramer (38–40). The EeAChE-specific peptide Ile^{418}–Gln^{446}, which is located between the very long helix $\alpha^4_{7,8}$ and the short strand β_8 of a subunit, protrudes at the surface of the subunit opposite the entrance of the active center gorge (5). Hence in tetramer A, the four Ile^{418}–Gln^{446} peptides are freely accessible to the solvent, an exposition that, along with the high flexibility imparted by the high content in Gly residues, likely accounts for the absence of density in these regions.

Structure B—In EeAChE structure B, the two dimers arrange as a compact, square nonplanar tetramer, also of a marked dimensional asymmetry (Fig. 3). Compared with structure A, the tetramer folds as to position the two four-helix bundle axes 60° from each other, and one dimer rotates relative to the second one by ~40° as to reorient the main axes of the two dimers antiparallel. At the dimer-dimer interface, which now extends in a direction perpendicular to the plane made by the two four-helix bundle axes, the facing loops $Cys^{256(257)}$–$Cys^{267(272)}$ are still separated by 13 Å, consistent with bridges possibly imparted by the facing oligosaccharide moieties linked to $Asn^{161(162)}$ and $Asn^{260(265)}$, and the four $Thr^{570(543)}$ residues, which are terminal to helices α_{10}, by 32 Å.

In tetramer B, the axes of the EeAChE active center gorges are oriented antiparallel within a dimer but are tilted by 120° from a dimer to the second one. Of the four peripheral sites, two, from diagonally opposed subunits, are exposed at the surface of the assembly and are freely accessible to the outside solvent; the two other peripheral sites, from the second pair of diagonally opposed subunits, face the tetramer internal space. A symmetric situation applies to the four peptides Ile^{418}–Gln^{446}, of which two are exposed to the outside solvent and are disordered and two face the internal space. As a result, residue Val^{447}, at the same position as mAChE-Ala^{420} in subunit *A* in the first dimer, is separated by 17 Å from peripheral site residues $Tyr^{336(341)}$ and $Trp^{281(286)}$ at the gorge entrance of subunit *C* in the second dimer. The presence of a weak, loop-shaped electron density in this region between subunits *A* and *C* suggests that, in the internal space, the peptide undergoes stabilizing interactions. The same weak density is observed between the peptide of subunit *D* and the peripheral site region of subunit *B*. Hence, in tetramer B, peptides Ile^{418}–Gln^{446} of two subunits may interact with the peripheral site regions of the facing two subunits, a situation reminiscent of the recently reported intersubunit interaction of mAChE loop Cys^{257}–Cys^{272}, also rich in Gly residues, with the facing peripheral site

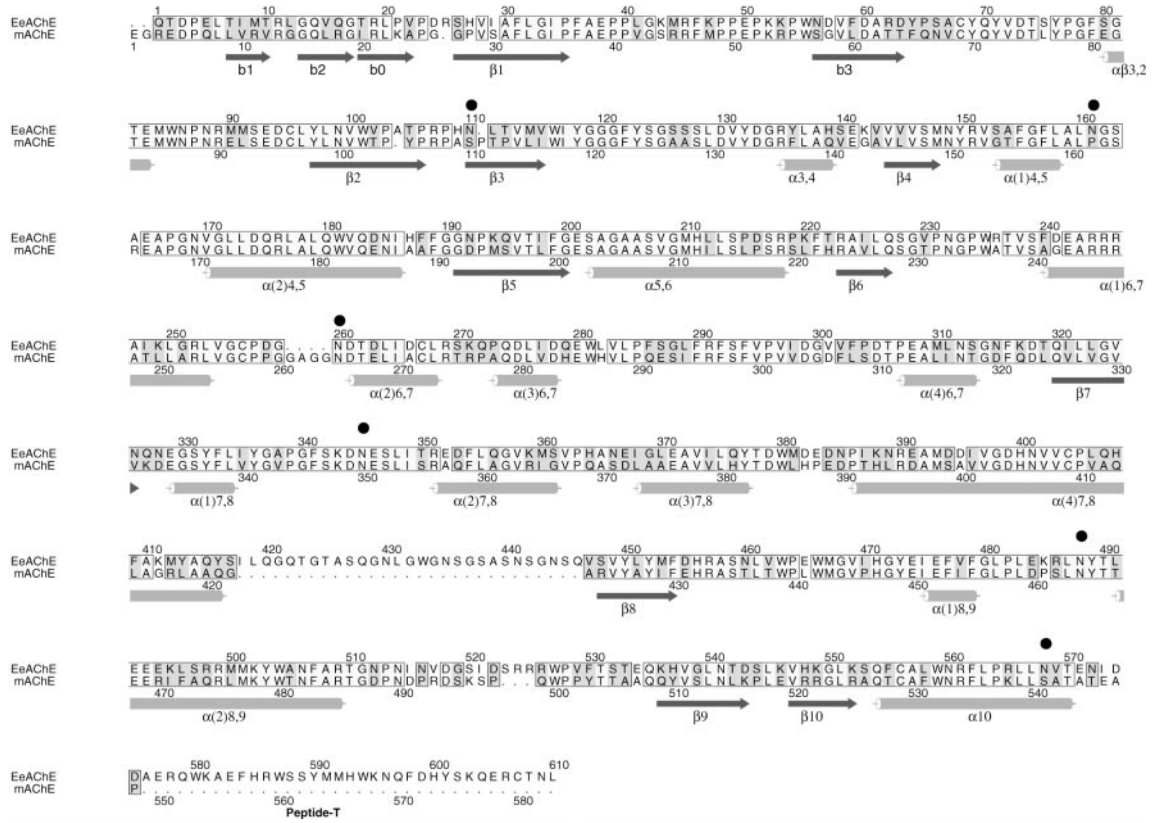

FIG. 2. **Alignment of the amino acid sequences of EeAChE and mAChE.** The secondary structure motifs of mAChE (12, 18) are specified according to Ref. 45. The putative *N*-glycosylation sites of EeAChE (5) are indicated by *black spheres*.

region (12). As a result, the surface area buried at the dimer-dimer interface is larger, and the space between the two dimers is 2-fold narrower than in tetramer A.

The Carboxyl-terminal T Peptides

The EeAChE carboxyl-terminal T peptide, $Glu^{571(544)}$–Leu^{610}, located in the extension of helix α_{10}, has no counterpart in the crystallized mAChE and TcAChE. Indeed, monomeric mAChE was generated as a soluble enzyme truncated after residue 548 (13), whereas dimeric TcAChE was enzymatically solubilized from a dimer of $AChE_H$ subunits (41). The T peptide, containing ~40 residues, of which nine are hydrophobic residues conserved among cholinesterases, was predicted to be organized as one or several helical regions forming one or two four-helix bundles (9, 10).

The amphipathic character of the T peptide precludes its full exposition to the solvent and total disorder. In addition, in contrast to the large surface area buried at the mAChE dimer-dimer interface (12), the limited surface areas buried at the dimer-dimer interfaces of the EeAChE tetramers appear insufficient for cohesion of the two dimers (42). These constraints, along with the large internal space observed in each of the two tetramers, raise the questions of the positions of the four T peptides in the EeAChE structures and of their contribution to the dimer-dimer interface. In the loose tetramer A, the four carboxyl-terminal T peptides could either be buried at the center of the arrangement, as proposed based on a square planar model for association of nonamphiphilic AChE subunits (10), or pair off and exit on either side of the tetramer plane, as recently suggested from analysis of the compact, pseudo-square planar tetramer of crystalline mAChE (12). In the folded, compact tetramer B, the four T peptides could be exposed on the same side of the arrangement, roughly similar to a recent model for tetrameric human butyrylcholinesterase (9). Either option would be expected to stabilize the four T peptides and provide the tetramer with the locking points, internal or external to the arrangement, that are required for dimer-dimer cohesion.

Actually, an additional density is apparent in the EeAChE structures, which is made of a loop-shaped portion located in the extension of helix α_{10} in the internal space and followed by a rod-shaped portion aligning antiparallel to helix α_{10}; the same density is found at the end of each of the four helices α_{10} and on either sides of each of the two four-helix bundles in tetramer A (Fig. 4). It is also found in the corresponding regions of tetramer B (not shown). The good fit of the mAChE carboxyl-terminal segment Ala^{544}–Ala^{547} into the loop-shaped portion and of a theoretical 10-residue α-helix into the rod-shaped portion suggests that this density represents the T peptide amino terminus up to (about) residue Phe^{584}. Hence, in a dimer, the amino termini of two T peptides pack against the dimer four-helix bundle, made of helices $\alpha^3{}_{7,8}$ and α_{10} from two subunits, perhaps to form a six-helix bundle. The orientation of the T peptide amino terminus appears to dictate the exit of the rest of the T peptide out of the tetramer in the extention of the bundle, where tiny density is detected. This suggests that the disulfide set that links one dimer with the residual tail and the disulfide that forms between monomers are distal to each other, a geometry consistent with the earliest models for AChE tetramers (*cf*. Fig. 11 in Ref. 4). In the crystallized EeAChE tetramers, however, some of the T peptides may be truncated carboxyl-terminal to residue Arg^{586} (*cf*. above); hence in the crystals, the residual T peptide amino-terminal parts may undergo stabilizing interactions that differ from those occurring in the physiological tetramer. Because of the current resolutions, second solutions of the two structures, alternative to tetramers A and B, might also be considered; however, the higher number of putative contacts at the dimer-dimer inter-

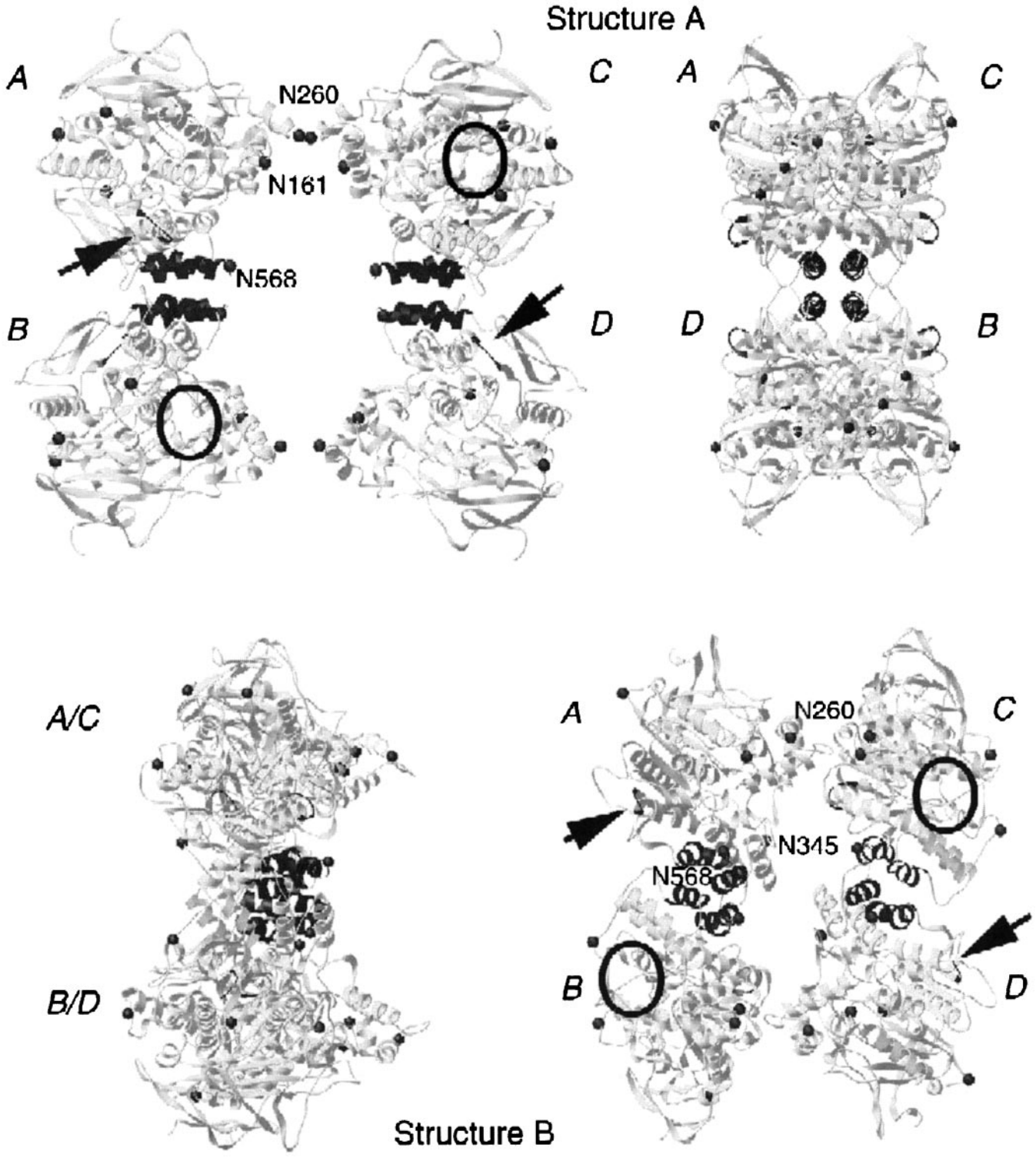

FIG. 3. **Overall views of the loose, pseudo-square planar EeAChE tetramer A and the compact, square nonplanar EeAChE tetramer B.** *Top left*, ribbon diagram of tetramer A viewed perpendicular to the four-helix bundle axis; *top right*, tetramer A viewed parallel to the four-helix bundle axis, 90° from the left view. *Bottom left*, ribbon diagram of tetramer B viewed perpendicular to the four-helix bundle axis of dimer *AB* (which is oriented as in the *top left panel* and is masked by dimer *CD*); *bottom right*, tetramer B viewed perpendicular to the dimer-dimer interface, 90° from the left view. The italicized labels *A* and *B* refer to the subunits in the left dimer and labels *C* and *D* to subunits in the right dimer for the *top left* and *bottom right* orientations. In tetramer A (overall dimensions: 132 × 132 × 55 Å), the main axes of the two dimers are tilted by ~40° from each other and the axes of the two four-helix bundles, made of helices $\alpha^3_{7,8}$ and α_{10} from two subunits and displayed in *black*, are aligned antiparallel with convergent helices α_{10}; the four peripheral sites, of which two from diagonally opposed subunits are oriented above the plane of the figure (*circled*), are accessible to the outside solvent; the apparent free space in the center of tetramer A is 75 Å long × 35 Å wide. In tetramer B (130 × 100 × 55 Å), the main axes of the two dimers are aligned antiparallel and the two four-helix bundle axes are positioned 60° from each other with convergent helices α_{10}; of the four peripheral sites, two are accessible to the outside solvent (*circled*) and two face the central, internal space (75 × 15 Å). For each of the two structures, the backbone shown is that of mAChE but residue numbering is that of EeAChE (*cf.* Fig. 2); the position of peptide Ile^{418}–Gln^{446}, which is unique to EeAChE and has not been modeled, is indicated by an *arrow*; the putative *N*-glycosylation sites are indicated by *black spheres*; and the labels N and C indicate the amino and carboxyl termini of subunit *A*, respectively.

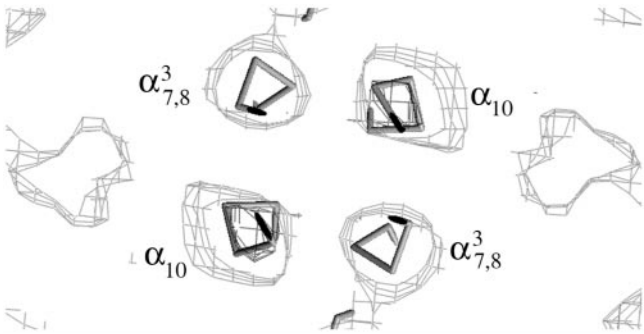

FIG. 4. **Cross-section of the electron density map in the four-helix bundle region.** Portions of the starting model (Cα atoms) are displayed in *black*. Shown in *gray* are the 4.5 Å resolution $2F_o$-F_c electron density map (contoured at 1.2σ) in the four-helix bundle region of dimer *AB* in tetramer A (*cf*. Fig. 3) and the F_o-F_c electron density map (contoured at 3σ) calculated using a starting model without helix α_{10} and visible at the center of this helix. The portions of density observed in the extension of helices α_{10} (not displayed) and on either sides of the four-helix bundle (made of helices $\alpha^3_{7,8}$ and α_{10} from subunits *A* and *B*) may represent the amino-terminal ends of the T peptides of these two subunits.

faces and striking resemblance with the subunit arrangement found in the mAChE structure (12) support tetramers A and B as the more convincing solutions.

A Flexible AChE Tetramer?

Overall, each of EeAChE tetramers A and B is consistent not only with the tetrameric arrangement of subunits of crystalline mAChE (12) but also with tetrameric arrangements observed *in situ* (*cf*. Fig. 2c in Ref. 6). Also, a structure similar to structure A but showing a larger tilt (by ~12°) of the two dimers in the tetramer was recently solved by Raves *et al.* (43) (Protein Data Bank code 1EEA) from a data set earlier collected on a crystal of the same space group as our form A crystals but different unit cell dimensions and grown from polyethylene glycol (16). The existence of two extreme conformational states of the EeAChE tetramer could be pH or/and temperature-dependent because the EeAChE form A crystals (as the form grown by Schrag *et al.* (16) and the mAChE crystals) were grown at pH $\geq$ 8 and at 4 °C, whereas the EeAChE form B crystals were grown at pH $\leq$ 6 and at 20 °C (*cf*. "Experimental Procedures" and Refs. 12 and 16). Yet, tetramer B should undergo a significant conformational transition into a state resembling tetramer A (or the 1EEA tetramer) to accomodate four molecules of the large peripheral site ligand, fasciculin (*cf*. Fig. 5 in Ref. 18), a transition expected to reposition residues at the dimer-dimer interface because the noncovalent intersubunit and fasciculin-EeAChE interactions are likely to differ substantially in affinity (*cf*. 12, 13, 18, 40). In fact, equilibrium analysis of EeAChE inhibition by increasing fasciculin concentrations in pH 5.5 and pH 9.0 buffers reveals complete inhibition curves reaching, at saturating fasciculin concentrations, the residual activity of the complex (*cf*. 13), consistent with occupancy of the tetramer four peripheral sites by fasciculin in solutions of either pH values.[3]

Conformational flexibility of the homologous 11S TcAChE species, evidenced by fluorescence polarization spectroscopy, was proposed to reflect motion of discrete segments of the tetramer molecule (segmental motion) rather than global rotation of the tetramer as a rigid macromolecule (44). Hence, structures A and B may correspond to distinct conformational states of an EeAChE tetramer undergoing, in solution, significant flexibility about the four-helix bundle axis and along the dimer-dimer interface axis. Most importantly, the possibility for several conformations of an overall tetrameric but malleable arrangement of AChE subunits would make the tetramer able to fit either of the carboxyl-terminal sequences, differing in length and amphipathic character, which characterize the diverse AChE molecular forms. Whether this flexibility is also related to regulation of catalysis is unknown. Because the high solvent content of the crystal forms used in this study precludes achievement of a higher resolution structure, even if synchrotron radiation were used, efforts to grow crystal forms of a higher diffraction potency are underway.

Acknowledgments—We thank Drs. Stéphanie Simon and Jean Massoulié (Ecole Normale Supérieure, Paris) for providing us with the cDNA-encoded sequence of EeAChE prior to publication and Dr. Palmer Taylor (UCSD, La Jolla) for critical review of the manuscript and fruitful discussions.

[3] P. Marchot, unpublished data.

REFERENCES

1. Massoulié, J., Pezzementi, L., Bon, S., Krejci, E., and Valette, F. M. (1993) *Prog. Neurobiol. (Oxf.)* **41,** 31–91
2. Taylor, P., and Radic, Z. (1994) *Annu. Rev. Pharmacol. Toxicol.* **34,** 281–320
3. Anglister, L., and Silman, I. (1978) *J. Mol. Biol.* **125,** 293–311
4. Lee, S. L., and Taylor, P. (1982) *J. Biol. Chem.* **257,** 12292–12301
5. Simon, S., and Massoulié, J. (1997) *J. Biol. Chem.* **272,** 33045–33055
6. Rieger, F., Bon, S., Massoulié, J., and Cartaud, J. (1973) *Eur. J. Biochem.* **34,** 539–547
7. Cartaud, J., Reiger, F., Bon, S., and Massoulié, J. (1975) *Brain Res.* **88,** 127–130
8. Cartaud, J., Bon, S., and Massoulié, J. (1978) *J. Cell Biol.* **77,** 315–322
9. Blong, R. M., Bedows, E., and Lockridge, O. (1997) *Biochem. J.* **327,** 747–757
10. Giles, K. (1997) *Protein Eng.* **10,** 677–685
11. Simon, S., Krejci, E., and Massoulié, J. (1998) *EMBO J.* **17,** 6178–6187
12. Bourne, Y., Taylor, P., Bougis, P. E., and Marchot, P. (1999) *J. Biol. Chem.* **274,** 2963–2970
13. Marchot, P., Ravelli, R. B. G., Raves, M. L., Bourne, Y., Vellom, D. C., Kanter, J., Camp, S., Sussman, J. L., and Taylor, P. (1996) *Protein Sci.* **5,** 672–679
14. Leuzinger, W., Baker, A. L., and Cauvin, E. (1968) *Proc. Natl. Acad. Sci. U. S. A.* **59,** 620–623
15. Chothia, C., and Leuzinger, W. (1975) *J. Mol. Biol.* **97,** 55–60
16. Schrag, J. D., Schmid, M. F., Morgan, D. G., Phillips, G. N., Jr., Chiu, W., and Tang, L. (1988) *J. Biol. Chem.* **263,** 9795–9800
17. Sussman, J. L., Harel, M., Frolow, F., Oefner, C., Goldman, A., Toker, L., and Silman, I. (1991) *Science* **253,** 872–879
18. Bourne, Y., Taylor, P., and Marchot, P. (1995) *Cell* **83,** 503–512
19. Grassi, J., Frobert, Y., Lamourette, P., and Lagoutte, B. (1988) *Anal. Biochem.* **168,** 436–450
20. Ellman, G. L., Courtney, K. D., Andres, V., Jr., and Featherstone, R. M. (1961) *Biochem. Pharmacol.* **7,** 88–95
21. Otwinowski, Z. (1993) in *Proceedings of the CCP4 Study Weekend on Data Collection and Processing* (Sawyer, L., Issacs, N., and Burley, S., eds) pp. 56–62, Science and Engineering Research Council/Daresbury Laboratory, Warrington, England
22. Evans, P. R. (1993) in *Proceedings of CCP4 Study Weekend on Data Collection and Processing* (Sawyer, L., Issacs, N., and Burley, S., eds) pp. 114–122, Science and Engineering Research Council/Daresbury Laboratory, Warrington, England
23. CCP4 Collaborative Computational Project No. 4 (1994) *Acta Crystallogr. Sect. D* **50,** 760–763
24. Matthews, B. W. (1968) *J. Mol. Biol.* **33,** 491–497
25. Navaza, J. (1994) *Acta Crystallogr. Sect. A* **50,** 157–163
26. Brünger, A. T., Adams, P. D., Clore, G. M., DeLano W. L., Gros, P., Grosse-Kunstleve, R. W., Jiang, J-S., Kuszewski, J., Nilges, M., Pannu, N. S., Read, R. J., Rice, L. M., Simonson, T., and Warren, G. L. (1998) *Acta Crystallogr. Sect. D* **54,** 905–921
27. Barton G. J. (1993) *Protein Eng.* **6,** 37–40
28. Carson, M. (1991) *J. Appl. Crystallogr.* **24,** 958–961
29. Roussel, A., and Cambillau, C. (1989) in *Silicon Graphics Geometry Partners Directory* (Silicon Graphics Committee, eds) pp. 77–78, Silicon Graphics, Mountain View, CA
30. Dudai, Y., and Silman, I. (1974) *Biochem. Biophys. Res. Commun.* **59,** 117–124
31. Rosenberry, T. L., Chen, Y. T., and Bock, E. (1974) *Biochemistry* **13,** 3068–3079
32. Krejci, E., Coussen, F., Duval, N., Chatel, J. M., Legay, C., Puype, M., Vandekerckhove, J., Cartaud, J., Bon, S., and Massoulié, J. (1991) *EMBO J.* **10,** 1285–1293
33. Krejci, E., Thomine, S., Boschetti, N., Legay, C., Sketelj, J., and Massoulié, J. (1997) *J. Biol. Chem.* **272,** 22840–22847
34. Taylor, P., Jones, J. W., and Jacobs, N. M. (1974) *Mol. Pharmacol.* **10,** 78–92
35. Ralston, J. C., Rush, R. S., Doctor, B. P., and Wolfe, A. D. (1985) *J. Biol. Chem.* **260,** 4312–4318
36. Harel, M., Kleywegt, G. J., Ravelli, R. B. G., Silman, I., and Sussman, J. L. (1995) *Structure* **3,** 1355–1366
37. Rachinsky, T. L., Camp, S., Li, Y., Ekström, J., Newton, M., and Taylor, P. (1990) *Neuron* **5,** 317–327
38. Marchot, P., Khélif, A., Ji, Y-H., Mansuelle, P., and Bougis, P. E. (1993) *J. Biol. Chem.* **268,** 12458–12467
39. Gentry, M. K., Moorad, D. R., Hur, R. S., Saxena, A., Ashani, Y., and Doctor,

B. P.(1995) *J. Neurochem.* **64,** 842–849
40. Remy, M. H., Frobert, Y., and Grassi, J. (1995) *Eur. J. Biochem.* **231,** 651–658
41. Sussman, J. L., Harel, M., Frolow, F., Varon, L., Toker, L., Futerman, A. H., and Silman, I. (1988) *J. Mol. Biol.* **203,** 821–823
42. Janin, J., Miller, S., and Chothia, C. (1990) *J. Mol. Biol.* **204,** 155–164
43. Raves, M. L., Giles, K., Schrag, J. D., Schmid, M. F., Phillips, G. N., Jr., Chiu, W., Howard, A. J., Silman, I., and Sussman, J. L. (1998) in *Structure and Function of Cholinesterases and Related Proteins* (Doctor, B. P., Taylor, P., Quinn, D. M., Rotundo, R. L., and Gentry, M. K., eds) pp. 351–356, Plenum Publishing Corp., New York
44. Berman, H. A., Yguerabide, J., and Taylor, P. (1985) *Biochemistry* **24,** 7140–7147
45. Cygler, M., Schrag, J., Sussman, J. L., Harel, M., Silman, I., Gentry, M. K., Doctor, B. P. (1993) *Protein Sci.* **2,** 366–382